Characterization of 3 PET Tracers for Quantification of Mitochondrial and Synaptic Function in Healthy Human Brain: ^{18}F-BCPP-EF, ^{11}C-SA-4503, and ^{11}C-UCB-J

Ayla Mansur[1,2], Eugenii A. Rabiner[1,3], Robert A. Comley[4], Yvonne Lewis[1], Lefkos T. Middleton[5], Mickael Huiban[1], Jan Passchier[1,2], Hideo Tsukada[6], and Roger N. Gunn[1,2], for the MIND-MAPS Consortium

[1]Invicro LLC, London, United Kingdom; [2]Division of Brain Sciences, Imperial College London, London, United Kingdom; [3]King's College London, London, United Kingdom; [4]Abbvie, North Chicago, Illinois; [5]Neuroepidemiology and Ageing Research Unit, Imperial College London, London, United Kingdom; and [6]Hamamatsu Photonics, Hamamatsu City, Shizuoka, Japan

Mitochondrial complex 1 is involved in maintaining brain bioenergetics; σ-1 receptor responds to neuronal stress; and synaptic vesicle protein 2A reflects synaptic integrity. Expression of each of these proteins is altered in neurodegenerative diseases. Here, we characterize the kinetic behavior of 3 PET radioligands—^{18}F-BCPP-EF, ^{11}C-SA-4503, and ^{11}C-UCB-J—for the measurement of mitochondrial complex 1, σ-1 receptor, and synaptic vesicle protein 2A, respectively, and determine appropriate analysis workflows for their application in future studies of the in vivo molecular pathology of these diseases. **Methods:** Twelve human subjects underwent dynamic PET scans with each radioligand, including associated arterial blood sampling. A range of kinetic models was investigated to identify an optimal kinetic analysis method for each radioligand and a suitable acquisition duration. **Results:** All 3 radioligands readily entered the brain and yielded heterogeneous uptake consistent with the known distribution of the targets. The optimal models determined for the regional estimates of volume of distribution were multilinear analysis 1 (MA1) and the 2-tissue-compartment model for ^{18}F-BCPP-EF, MA1 for ^{11}C-SA-4503, and both MA1 and the 1-tissue-compartment model for ^{11}C-UCB-J. Acquisition times of 70, 80, and 60 min for ^{18}F-BCPP-EF, ^{11}C-SA-4503, ^{11}C-UCB-J, respectively, provided good estimates of regional volume of distribution values. An effect of age was observed on ^{18}F-BCPP-EF and ^{11}C-UCB-J signal in the caudate. **Conclusion:** These ligands can be assessed for their potential to stratify patients or monitor the progression of molecular neuropathology in neurodegenerative diseases.

Key Words: kinetic modeling; neurodegeneration; synapses; mitochondria; endoplasmic reticulum

J Nucl Med 2020; 61:96–103
DOI: 10.2967/jnumed.119.228080

The complex and heterogeneous pathophysiology of neurodegenerative diseases represents a major challenge for the discovery and development of disease-modifying therapeutics. A growing body of literature implicates cellular stress-related mitochondrial and endoplasmic reticulum (ER) dysfunction and related synaptic abnormalities as a common denominator across neurodegenerative diseases, making the mitochondrial/ER/synaptic axis an attractive system to target in the search for biomarkers that can be used to monitor disease progression (*1–3*). Mitochondrial adenosine triphosphate production is critical for the bulk of neuronal processes, including neurotransmitter synthesis and synaptic plasticity. The mitochondrial complex 1 (MC1) is a crucial component of this process, as it is where the first step of oxidative phosphorylation takes place (*4*). MC1 is responsible for cellular housekeeping mechanisms, including maintaining cellular calcium homeostasis, producing reactive oxygen and nitrogen species, and regulating apoptosis (*4*). Altered MC1 function has been associated with cell toxicity, accelerated aging, and the pathogenesis of multiple neurodegenerative diseases (*1*). In vivo quantification of MC1 in the brain has been made possible by the development of the PET radioligand ^{18}F-BCPP-EF (2-tert-butyl-4-chloro-5-{6-[2-(2-^{18}F-fluoroethoxy)-ethoxy]-pyridin-3-ylmethoxy}-2H-pyridazin-3-one) (*5*). Characterization of ^{18}F-BCPP-EF kinetics in the nonhuman primate brain has suggested its suitability for human evaluation, but no human data have been published to date (*6,7*).

A second regulator of cellular energy is the σ-1 receptor (σ1R), which is a chaperone protein that stabilizes the inositol phosphate 3 receptor voltage-dependent anion channel in the mitochondria-associated ER membrane (*8*). This channel is the principal pathway for calcium influx from the ER stores to the mitochondrion, with adenosine triphosphate production rate depending significantly on calcium concentration (*9*). σ1R is involved in synaptic plasticity and neuroprotection, with human postmortem evidence of altered expression in Alzheimer disease (*10–12*). Early PET imaging studies have used the radioligand ^{11}C-SA-4503 (^{11}C-labeled 1-[2-(3,4-dimethoxyphenthyl)]-4-(3-phenylpropyl)-piperazine dihydrochloride) to evaluate σ1R status in healthy, Parkinson disease, and Alzheimer disease cohorts, though an evaluation of the optimal imaging methodology for ^{11}C-SA-4503 has yet to be established (*13–15*).

The synaptic vesicle protein A (SV2A) is a membrane glycoprotein expressed ubiquitously on synaptic vesicles in presynaptic terminals and regulates calcium-mediated neurotransmitter release (*16*). SV2A has a stable synaptic stoichiometry with good correlation to recognized synaptic density markers such as synaptophysin and thus offers great promise as a marker of synaptic terminal density in the human brain (*17*). Synaptic loss is central to all neurodegenerative disease pathology, with evidence of changes to presynaptic structure and function in presymptomatic stages of disease, raising interest

Received Mar. 5, 2019; revision accepted Jun. 4, 2019.
For correspondence or reprints contact: Ayla Mansur, Imperial College London, Hammersmith Hospital London, 22 Du Cane Rd., London W12 0NN, U.K.
E-mail: ayla.mansur@invicro.co.uk
Published online Jul. 19, 2019.

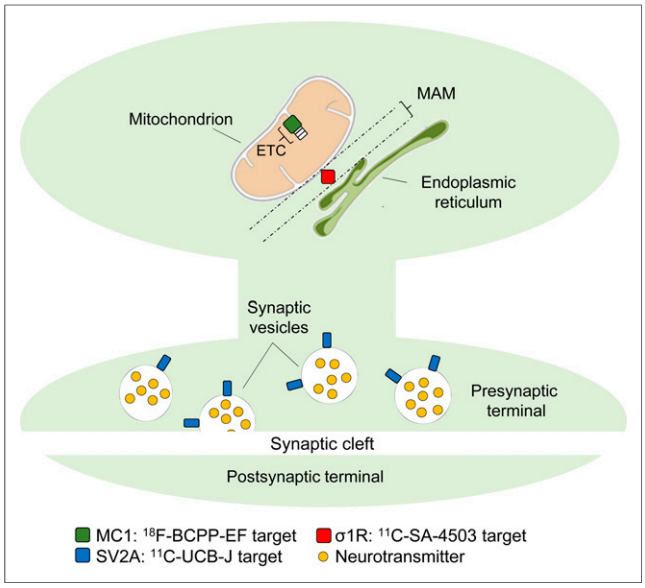

FIGURE 1. Mitochondrial/ER/synaptic axis. ETC = electron transport chain; MAM = mitochondria-associated endoplasmic reticulum membrane.

in the use of SV2A markers (*18–20*). Quantification of SV2A has been made possible by the discovery of the radioligand ^{11}C-UCB-J ((*R*)-1-((3-(^{11}C-methyl-^{11}C)pyridin-4-yl)methyl)-4-(3,4,5-trifluorophenyl)pyrrolidin-2-one), with recent findings indicating a reduction in ^{11}C-UCB-J–specific binding in healthy aging, mild cognitive impairment, and Alzheimer disease (*21–23*).

The availability of the PET radioligands ^{18}F-BCPP-EF, ^{11}C-SA4503, and ^{11}C-UCB-J enables the quantification of MC1, σ1R, and SV2A, respectively, and allows us to test the hypothesis that a combination of these markers could provide a useful index of the function of the mitochondrial/ER/synaptic axis depicted in Figure 1.

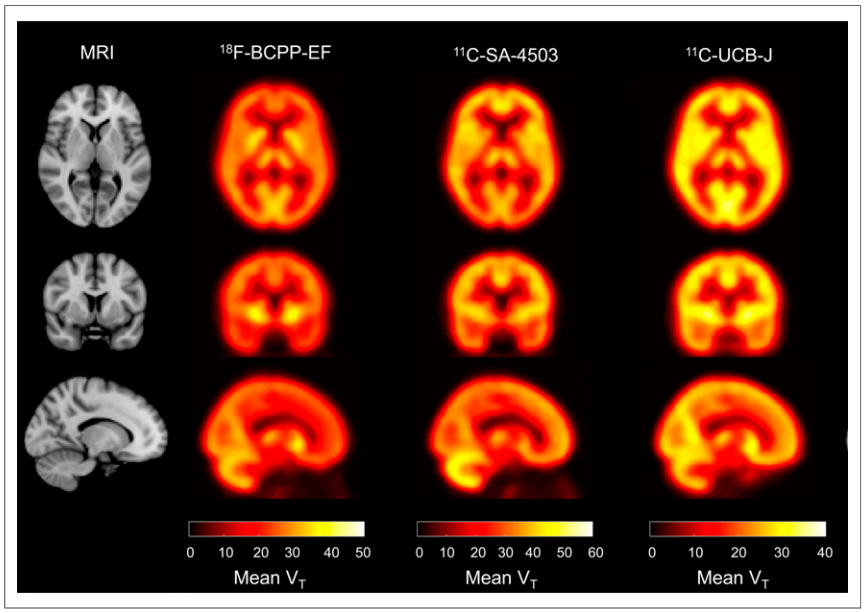

FIGURE 2. Orthogonal cross-sections of average parametric V_T images generated by 1TC (^{11}C-UCB-J) and Logan graphical analysis (^{11}C-SA-4503 and ^{18}F-BCPP-EF).

The data utilized in this article were collected as part of ongoing studies funded by the MIND-MAPS consortium (www.invicro.com/mindmaps). The methods identified here will be used for the future quantification of healthy volunteer and patient cohorts in the MIND-MAPS program. The primary aim is to establish an appropriate set of image analysis workflows including optimal tracer kinetic quantification approaches and outcome measures for ^{18}F-BCPP-EF, ^{11}C-SA-4503, and ^{11}C-UCB-J in humans. A secondary aim is to explore whether MC1, σ1R, and SV2A expression is altered in healthy aging.

MATERIALS AND METHODS

Study Design

All procedures were in accordance with the ethical standards of East of England Cambridge South Research Ethics Committee. Twelve healthy volunteers (7 men/5 women, 61 ± 20 y old, range, 33–75 y) were screened and scanned at Invicro London's Hammersmith Hospital site. Each subject underwent structural MRI and 1 dynamic PET scan with ^{18}F-BCPP-EF, ^{11}C-SA-4503, and ^{11}C-UCB-J. Written informed consent was obtained from all subjects.

Radiotracer Synthesis

^{18}F-BCPP-EF, ^{11}C-SA-4503, and ^{11}C-UCB-J were synthesized as previously described (*5,24,25*). Injected dose information for each radioligand is summarized in Supplemental Table 1 (supplemental materials are available at http://jnm.snmjournals.org).

PET Acquisition

All PET scans were acquired on either a Hi-Rez Biograph 6 or a Biograph 6 TruePoint PET/CT scanner (Siemens Healthcare), with subjects receiving all 3 PET scans on the same scanner. A low-dose CT scan (30 mAs, 130 keV, 0.55 pitch) was performed immediately before each PET scan to estimate attenuation. An intravenous cannula was inserted into a cubital or forearm vein for radioligand administration, and a second cannula was inserted into the radial artery to enable arterial blood collection. The radioligands were administered as a bolus (20 mL over 20 s) at the start of the PET scan. Dynamic emission data were acquired over 90 min after radiotracer administration and were reconstructed into 26 frames (frame durations: 8 × 15 s, 3 × 60 s, 5 × 120 s, 5 × 300 s, and 5 × 600 s) using discrete inverse Fourier transform reconstruction. Corrections were applied for attenuation, randoms, and scatter.

Arterial Blood Acquisition

Whole-blood activity was measured using a continuous automatic blood sampling system (Allogg AB) at a rate of 5 mL/min for the first 15 min of the scan. Discrete blood samples were taken at 10, 15, 20, 25, 30, 40, 50, 60, 70, 80, and 90 min after the start of the scan, and total-blood and plasma radioactivity concentration was evaluated in in a Perkin Elmer 1470 10-well γ-counter. The fraction of plasma radioactivity constituted by unchanged parent radioligand (plasma parent fraction, or *ppf*) was determined using high-performance liquid chromatography. The plasma free fraction (f_p) was measured by ultrafiltration in triplicate using an arterial blood sample taken before tracer injection.

MR Acquisition

Each subject underwent a T1-weighted MRI scan for coregistration with PET images.

Scans were acquired on a Siemens 3-T Trio clinical MRI scanner (Siemens Healthineers) with a 32-channel phased-array head coil using a 3-dimensional magnetization-prepared rapid gradient echo sequence (echo time, 2.98 ms; repetition time, 2,300 ms; flip angle, 9°; voxel size, 1.0 × 1.0 × 1.0 mm).

Image Analysis and Processing

All image data were analyzed using Invicro London's in-house PET data quantification tool, MIAKAT (version 4.3.7), which implements MATLAB (version R2016a; MathWorks Inc.) and FSL (version 5.0.4; FMRIB) functions for brain extraction and SPM12 (Wellcome Trust Centre for Neuroimaging) for image segmentation and registration (*26*).

Each subject's MR images underwent brain extraction, gray matter segmentation, and rigid-body coregistration to a standard reference space (*27*). The template brain image and associated Center for Integrative Connectomics neuroanatomic atlas was then nonlinearly warped to the individual subject's MR images, on which the following regions of interest (ROIs) were defined: brain stem, substantia nigra, thalamus, ventral striatum, caudate, putamen, hippocampus, insular cortex, temporal lobe, parietal lobe, frontal cortex, and cerebellum (*28*). A centrum semiovale ROI was also generated from the automated anatomic labeling template as defined previously for investigation as a reference region for ^{11}C-UCB-J (*21,29*). PET images were registered to each subject's MR image and corrected for motion using frame-to-frame rigid-body registration. Regional time–activity curves were generated for each ROI.

Arterial Input Function Modeling

Optimal *ppf* models were identified for each tracer and applied to the total plasma activity curve to derive a metabolite-corrected arterial input function.

Tracer Kinetic Modeling

All time–activity curves were fitted with a 1-tissue-compartment (1TC) model, a 2-tissue-compartment (2TC) model, and multilinear analysis 1 (MA1) to estimate the total volume of distribution (V_T) (*30*). MA1 was applied to time–activity curve data, with integration intervals computed over 30–90 min for all tracers based on an initial assessment of an appropriate temporal window. Blood volume fraction was fixed to 5%. V_T/f_p was also assessed as an outcome measure to explore its utility in studies in which there are differences in f_p.

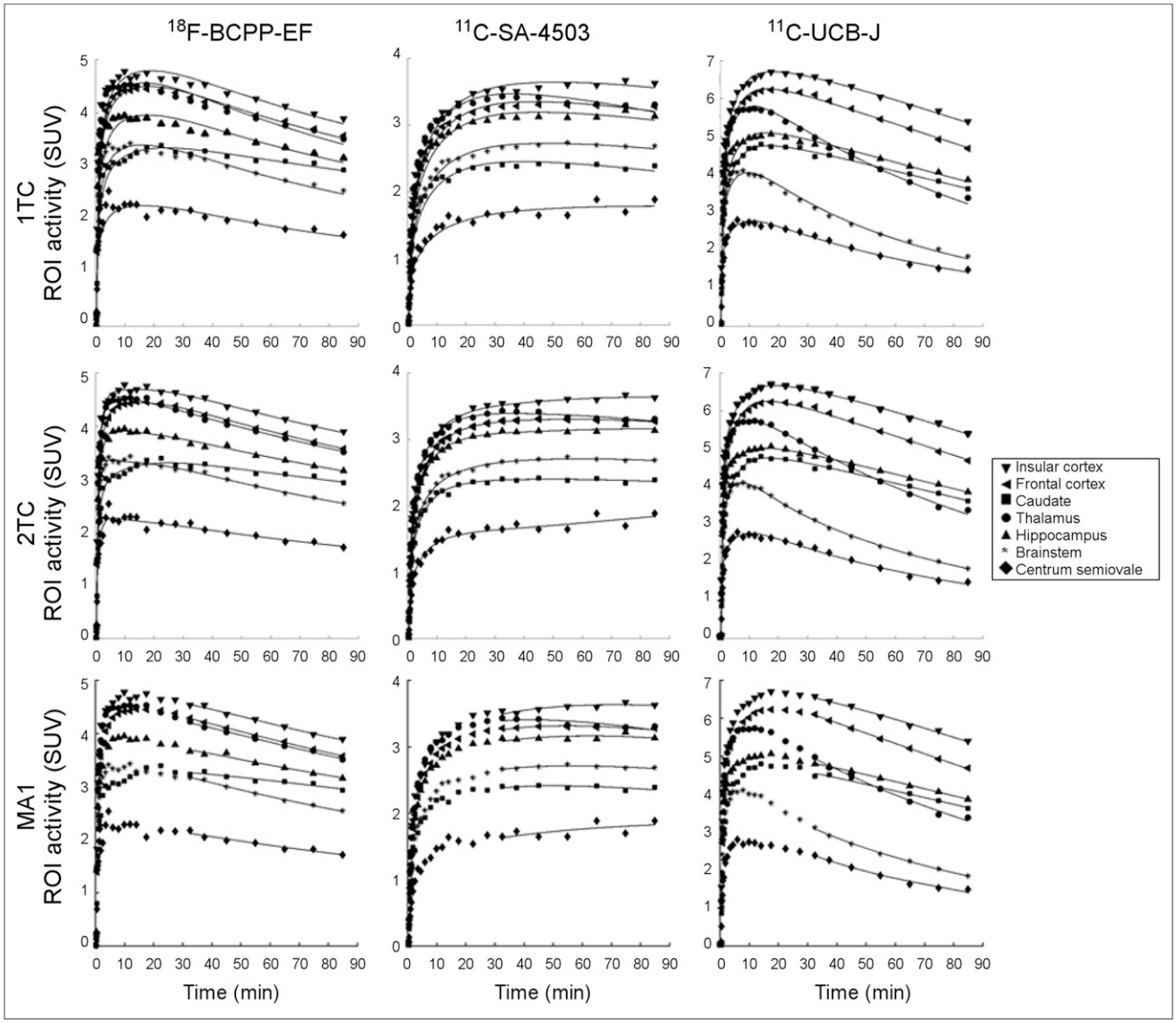

FIGURE 3. Representative model fits for ^{18}F-BCPP-EF, ^{11}C-SA-4503, and ^{11}C-UCB-J.

TABLE 1
V_T and $\%Vol_{roi}$ Estimates

Radioligand	Kinetic model	ROI												
		Centrum semiovale	Brain stem	Substantia nigra	Thalamus	Ventral striatum	Caudate	Putamen	Hippocampus	Insular cortex	Temporal lobe	Parietal lobe	Frontal cortex	Cerebellum
^{18}F-BCPP-EF	1TC	10.8	16.2	19.2	21	29.6	19.2	31.9	19.6	24.9	23.1	24.5	23.3	28.5
		19%	17%	14%	21%	21%	32%	20%	19%	18%	18%	21%	19%	17%
	2TC	11.9	17.5	20.9	22.8	31.6	20.4	34.1	21.6	26.5	24.7	26	24.7	30.6
		17%	17%	14%	20%	20%	32%	18%	18%	17%	17%	20%	18%	16%
	MA1	11.9	17.5	20.9	22.9	31.6	20.4	34	21.7	26.6	24.8	26.1	24.8	30.6
		17%	17%	14%	20%	20%	32%	19%	18%	17%	17%	20%	19%	16%
^{11}C-SA-5403	1TC	23.2	31.7	30.5	28.6	34	22	37.4	32.5	39.4	35.7	33	34.6	41.7
		23%	18%	17%	21%	21%	31%	18%	16%	15%	16%	18%	23%	17%
	2TC	26.5	37.9	34	32.7	36.8	29.4	43.8	37.9	45.9	41.5	37.7	39.4	47.7
		31%	22%	17%	22%	19%	26%	17%	15%	16%	16%	19%	23%	19%
	MA1	29.1	36.5	34.6	31.9	37.9	25.1	42.1	37	44.6	40.4	36.7	38.4	46.5
		29%	20%	21%	21%	21%	28%	16%	14%	16%	16%	18%	23%	18%
^{11}C-UCB-J	1TC	5.7	7.2	8.5	11.2	20.9	12.4	20.9	13.4	20.5	17.6	15.5	14	15.9
		12%	12%	10%	16%	13%	28%	11%	13%	10%	10%	14%	14%	10%
	2TC	5.9	7.4	8.9	11.4	21.2	12.6	21.1	14.6	20.9	19.3	18	17.7	16.5
		11%	11%	10%	15%	12%	28%	11%	12%	9%	9%	14%	13%	9%
	MA1	5.8	7.4	8.8	11.5	21.2	12.6	21.1	14.6	20.9	19.3	18	17.7	16.5
		12%	11%	9%	15%	12%	28%	10%	13%	9%	9%	13%	13%	9%
$\%Vol_{roi}$		0.11	2.33	0.07	1.38	0.15	0.46	0.62	0.50	0.83	8.00	6.28	5.39	6.49
		10%	5%	7%	5%	6%	11%	7%	9%	9%	6%	9%	9%	7%

Data are mean and COV.17 values for ^{11}C-SA-4503 2TC estimation; 3 values for ^{11}C-UCB-J 2TC estimation were excluded based on V_T of SE% $>$ 10.

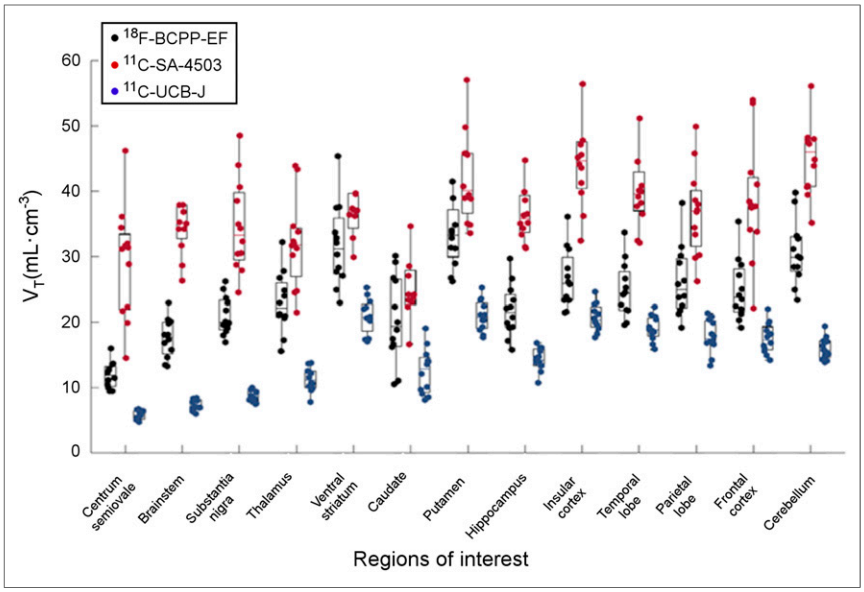

FIGURE 4. Distribution of regional V_T estimates.

Given the low white matter uptake we observed for ^{18}F-BCPP-EF, ^{11}C-SA-4503, and ^{11}C-UCB-J, we assessed the centrum semiovale as a pseudo reference region for each ligand and used it to calculate the distribution volume ratio (DVR).

Model Comparison and Selection

The performance of 1TC and 2TC models was assessed by the Akaike information criterion and parameter identifiability based on the percentage SE derived from the covariance matrix (*31*). Linear regression correlation coefficients (r^2) were used to compare performance between the graphical method MA1 and the compartmental models. V_Ts that were poorly estimated (SE% $>$ 10) were excluded from model comparisons.

Time Stability Analysis

The stability of each radioligand over time was evaluated by exploring the performance of the tracer kinetic models for varying scan lengths. The estimated V_Ts were expressed as percentages of the V_T estimated from the full 90-min scan. These analyses were aggregated together over all subjects, enabling assessment of the time stability of the radiotracers in the population.

Assessment of Age Effects on Outcome Measures

The effects of healthy aging on MC1, σ1R, and SV2A density were assessed using correlation analysis, with age as the predictor variable and the PET outcome measures and ROI volume as parameters of interest. ROI volume was normalized to whole-brain volumes:

$$\%Vol_{roi} = 100 \times \frac{Vol_{roi}}{Vol_{brain}}, \qquad \text{Eq. 1}$$

where Vol_{roi} is the volume in a given ROI and Vol_{brain} is the whole-brain volume. Percentage rates of change per year in V_T, V_T/f_p, DVR, and $\%Vol_{roi}$ were then calculated as

$$\%\Delta/\text{year} = 100 \times \left(\frac{\Delta\text{parameter}}{\Delta\text{age}}\right) \Big/ \text{parameter}_{\text{mean}}. \qquad \text{Eq. 2}$$

RESULTS

All participants completed three 90-min dynamic PET scans including arterial blood sampling and MRI. A summary of demographic information and individual scan parameters is included in Supplemental Table 1.

Arterial Input Function Modeling

Ppf data for ^{18}F-BCPP-EF were best described by a sigmoid model with 20% ± 8% intact parent radiotracer at 90 min. ^{11}C-SA-4503 metabolite data were best described by an exponential function in which *ppf* was estimated at 91% ± 5% at 90 min. ^{11}C-UCB-J metabolite data were described by a sigmoid model with approximately 25% ± 5% at 90 min. Individual *ppf* and input function profiles are shown in the Supplemental Figure 1.

Tracer Kinetic Modeling

All 3 tracers entered the brain readily and demonstrated a heterogeneous distribution (Fig. 2). ^{18}F-BCPP-EF uptake was fast, and peak SUVs were reached at about 5–12 min after injection. ^{11}C-SA-4503 uptake was slow and peaked at about 30–60 min after injection. ^{11}C-UCB-J displayed fast kinetics producing a peak SUV at about 7–21 min after injection.

All kinetic models reached convergence in the ^{18}F-BCPP-EF–derived regional time–activity curve data (Fig. 3). V_T was robustly estimated in all ROIs using both 1TC and 2TC, with the Akaike information criterion analysis favoring the 2TC over the 1TC. As 2TC- and MA1-derived V_T were in excellent agreement (r^2 = 0.99) (Supplemental Fig. 2A), both were chosen as suitable modeling methods for ^{18}F-BCPP-EF.

For ^{11}C-SA-4503, 2TC produced the most parsimonious fits to time–activity curves in 155 of the 156 tested cases as determined by the Akaike information criterion when compared with 1TC; however, V_T was poorly estimated in 17 of 156 cases. MA1 produced good fits to the time–activity curve data, and V_T estimates were in close agreement with those reliably estimated using the 2TC model (r^2 = 0.97) (Supplemental Fig. 2B) and were therefore chosen as the appropriate kinetic model.

All 3 models produced excellent fits to ^{11}C-UCB-J time–activity curve data. The Akaike information criterion preferred 2TC

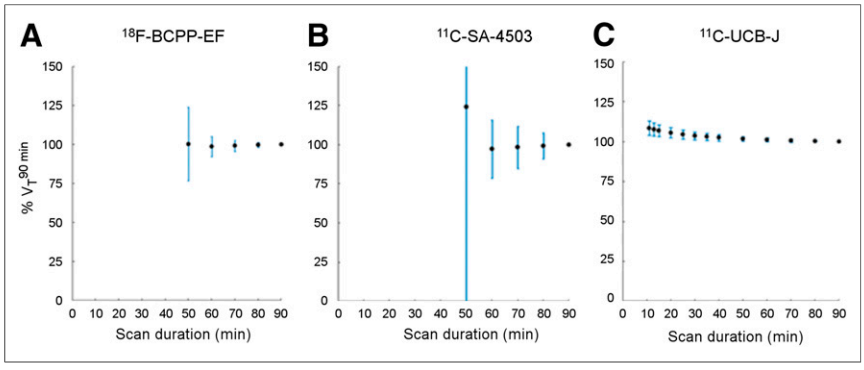

FIGURE 5. Time stability plots for ^{18}F-BCPP-EF (A), ^{11}C-SA-4503 (B), and ^{11}C-UCB-J V_T (C). First 50 min for ^{18}F-BCPP-EF and ^{11}C-SA-4503 have been excluded for clarity.

TABLE 2
Age Effects on Volumetric and PET Outcome Measures

ROI	$\%Vol_{roi}$			^{18}F-BCPP-EF			^{11}C-SA-4503			^{11}C-UCB-J		
	r	*P*	Δ/y	*r*	*P*	Δ/y	*r*	*P*	Δ/y	*r*	*P*	Δ/y
Centrum semiovale	0.26	0.42	0.2	−0.03	0.92	−0.05	0.02	0.95	0.05	−0.13	0.68	−0.13
Brain stem	0.14	0.65	0.05	−0.16	0.63	−0.21	−0.22	0.49	−0.35	−0.44	0.15	−0.41
Substantia nigra	−0.33	0.29	−0.17	0.02	0.94	0.03	−0.38	0.23	−0.62	−0.36	0.25	−0.28
Thalamus	0.16	0.62	0.07	−0.46	0.13	−0.74	−0.29	0.36	−0.49	−0.74	0.01*	−0.93
Ventral striatum	−0.18	0.57	−0.09	−0.25	0.44	−0.39	−0.24	0.45	−0.4	−0.62	0.03*	−0.63
Caudate	0.46	0.14	0.39	−0.65	0.02*	−1.68	−0.35	0.26	−0.77	−0.82	0.001†	−1.83
Putamen	−0.51	0.09	−0.27	−0.14	0.67	−0.21	−0.02	0.94	−0.03	−0.44	0.16	−0.39
Hippocampus	−0.48	0.11	−0.33	−0.27	0.4	−0.39	−0.17	0.6	−0.19	−0.61	0.04*	−0.59
Insular cortex	−0.41	0.19	−0.28	−0.26	0.41	−0.35	−0.21	0.52	−0.26	−0.6	0.04*	−0.48
Temporal lobe	−0.71	0.01*	−0.51	−0.26	0.42	−0.35	−0.2	0.54	−0.25	−0.55	0.06	−0.44
Parietal lobe	−0.77	0.003†	−0.36	−0.32	0.31	−0.52	−0.17	0.61	−0.24	−0.61	0.03*	−0.69
Frontal cortex	−0.75	0.01*	−0.53	−0.35	0.27	−0.52	−0.23	0.47	−0.43	−0.65	0.02*	−0.69
Cerebellum	−0.45	0.14	−0.25	0.02	0.96	0.02	−0.23	0.47	−0.33	−0.13	0.68	−0.11

*$P < 0.05$.
†$P < 0.005$.

over 1TC in 146 of 156 cases; however, 3 of 156 V_T estimates were unstable with 2TC. MA1 produced good fits that were well correlated with 1TC fits ($r^2 = 0.99$) (Supplemental Fig. 2C).

All V_T estimates are summarized in Table 1. The average coefficient of variance (COV) of V_T across all regions investigated was 19% ± 4% for ^{18}F-BCPP-EF, 20% ± 6% for ^{11}C-SA-4503, and 13% ± 5% for ^{11}C-UCB-J (Fig. 4). There was no relationship between injected mass and V_T for any of the radioligands (Supplemental Table 2).

Time Stability Analysis

For ^{18}F-BCPP-EF, 70 min of PET data provided good stability of V_T (Fig. 5A), with the resulting V_T being 98.4% ± 6.7% of the final V_T. An 80-min acquisition with ^{11}C-SA-4503 produced reliable V_T estimates that were 98.2% ± 1.2% of the V_T estimated from the full 90-min scan (Fig. 5B). ^{11}C-UCB-J estimates derived from a 60-min scan were 98.0% ± 1.8% of the V_T estimated from the full 90-min scan (Fig. 5C). Regional time stability analyses are included in Supplemental Figures 3–5.

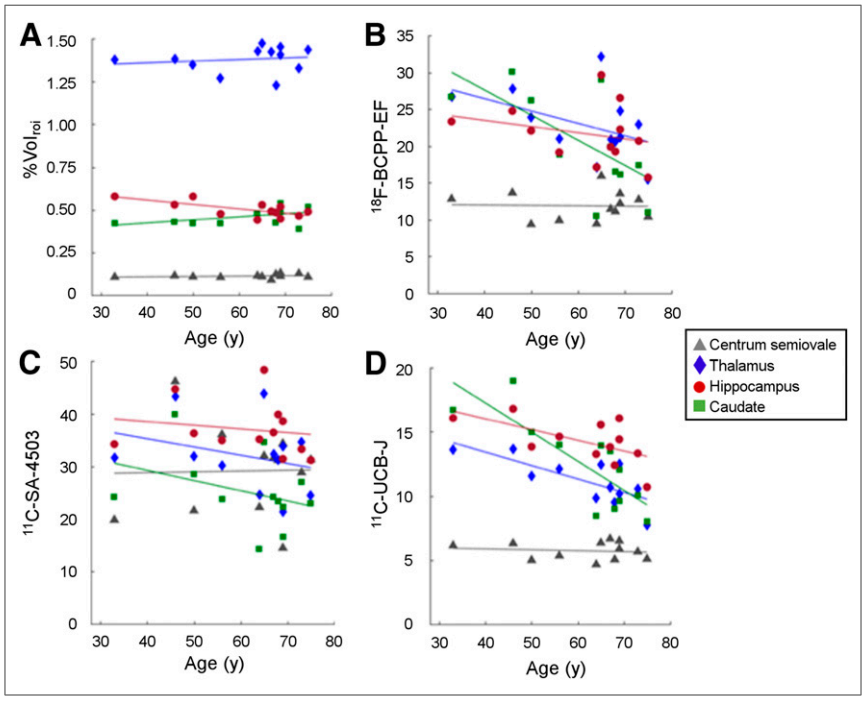

FIGURE 6. Linear regression plots of age vs. $\%Vol_{roi}$ (A), ^{18}F-BCPP-EF V_T (B), ^{11}C-SA-4503 V_T (C), and ^{11}C-UCB-J V_T (D).

Assessment of DVR and V_T/f_p as Outcome Measures

DVR results were less variable between subjects than were the corresponding V_T estimates except for ^{11}C-SA-4503, for which DVR results were more susceptible to individual differences than were the V_T estimates (Supplemental Table 3). Correction of V_T by f_p had no significant effect on intersubject variability for any of the ligands (Supplemental Table 4).

Assessment of Age Effects on Outcome Measures

We observed a statistically significant yearly reduction in volume of 0.52%, 0.36%, and 0.53% in the temporal lobe, parietal lobe, and frontal cortex, respectively (Table 2; Fig. 6A).

^{18}F-BCPP-EF V_T decreased with age in most regions, with the highest reduction—1.68%/y—being in the caudate (Fig. 6B). A similar negative trend was observed for ^{11}C-SA-4503; however, none of the correlations reached significance (Fig. 6C). ^{11}C-UCB-J V_T was negatively correlated with age in all regions, with significant reductions in the

thalamus, ventral striatum, caudate, insula, parietal lobe, and frontal cortex (Fig. 6D; Table 2).

The results of our regression analysis between DVR and age were similar to those observed with V_T (Supplemental Fig. 6A; Supplemental Table 5). ^{18}F-BCPP-EF V_T/f_p was negatively correlated with age in the thalamus, caudate, and parietal lobe, whereas correcting ^{11}C-UCB-J V_T by f_p masked any prior age effects on SV2A density except in the caudate (Supplemental Fig. 6B; Supplemental Table 6). Lastly, ^{11}C-UCB-J f_p appeared to decrease with age, though this difference did not reach statistical significance (Supplemental Fig. 7).

DISCUSSION

The current study evaluated a variety of kinetic quantification approaches for the radioligands ^{18}F-BCPP-EF, ^{11}C-SA-4503, and ^{11}C-UCB-J in the human brain. In addition, we examined the effects of age on the density of MC1, σ1R, and SV2A. ^{18}F-BCPP-EF displayed reversible kinetics, with the highest uptake being observed in striatal regions, consistent with nonhuman primate data (*7*). ^{18}F-BCPP-EF metabolism was rapid, and the kinetics were well described using both MA1 and 2TC. Our results showed a reduction in ^{18}F-BCPP-EF signal with age, in line with preclinical experiments (*5*). Importantly, reductions in the caudate did not appear to be driven by changes in volume (Figs. 6A and 6B), suggesting that striatal mitochondrial density could be particularly susceptible to aging.

The tracer characteristics of ^{11}C-SA-4503 agreed with initial results in humans (*13*). We selected MA1 as the optimal model to describe ^{11}C-SA-4503 kinetics because approximately 11% of our 2TC-derived V_T estimates were poorly estimated. This was mainly due to the poor estimation of k_4 in the caudate, substantia nigra, and centrum semiovale, suggesting that ^{11}C-SA-4503 kinetics approach irreversibility in these regions and should be interpreted with caution. ^{11}C-SA-4503 signal was highest in the cerebellum, consistent with previous mouse and initial human studies (*13,24*). We observed an age-related decrease in ^{11}C-SA-4503 signal consistent with preclinical data, though this difference did not reach significance (*32*).

^{11}C-UCB-J uptake was widespread and displayed fast kinetics that were well described by all 3 models, in agreement with previous reports (*21*). Given the near-perfect correlation between MA1- and 1TC-derived V_T estimates, we suggest using either 1TC or MA1 for ^{11}C-UCB-J quantification. Consistent with recent reports of age effects on ^{11}C-UCB-J binding, we observed an effect of age on SV2A density in the caudate, where the reduction in signal remained significant after correction by f_p (*22*). Age effects on V_T remained significant for most regions after controlling for age effects on *%Vol* (Supplemental Table 7).

Comparison of V_T estimates within and between groups requires the measured f_p for a particular radioligand to be unchanged between subjects or experimental conditions. In our dataset, we observed a negative effect of age on f_p for ^{11}C-UCB-J ($r^2 = -0.3$, $P = 0.10$) (Supplemental Fig. 7). We therefore took V_T/f_p as the primary outcome measure. Future ^{11}C-UCB-J studies should evaluate f_p and correct for any potential differences, especially when studying patient groups.

Ideally, nondisplaceable binding can be directly estimated from a reference region, which is not feasible with compounds lacking a region devoid of any binding. The use of DVR provides a partial solution to this problem by relying on a region with low specific binding, eliminating some of the intersubject variability in the estimation of individual input functions. Although no known reference region exists for ^{18}F-BCPP-EF, we found that V_T estimates were about 50% lower in the centrum semiovale than in gray matter regions. ^{11}C-UCB-J V_T estimates were about 60% lower in the centrum semiovale than in gray matter regions, supporting previous suggestions of its potential use as a reference region for ^{11}C-UCB-J (*33*). Blocking studies with specific MC1 and SV2A compounds should be conducted in both healthy and disease cohorts to confirm the viability of the centrum semiovale as a reference region. ^{11}C-SA-4503 V_T was not significantly lower in white matter than in gray matter regions, making DVR an unsuitable outcome measure for this tracer.

On the basis of our time stability analyses, we conclude that scanning for at least 70, 80, and 60 min is sufficient to reliably estimate V_T from a ^{18}F-BCPP-EF, ^{11}C-SA-4503, and ^{11}C-UCB-J scan, respectively. Our ^{11}C-UCB-J time stability results support those from a recent test–retest analysis of ^{11}C-UCB-J kinetics (*34*).

CONCLUSION

We have established a set of optimal tracer kinetic quantification models and outcome measures for ^{18}F-BCPP-EF, ^{11}C-SA-4503, and ^{11}C-UCB-J in the healthy human brain. We suggest that MA1 or 2TC can be used to quantify ^{18}F-BCPP-EF, that MA1 should be used to quantify ^{11}C-SA-4503, and that both MA1 and 1TC are suitable for ^{11}C-UCB-J quantification. Lastly, our analysis of the effect of age on this dataset suggests that ^{18}F-BCPP-EF and ^{11}C-UCB-J signal in the caudate might serve as a marker of age-related mitochondrial dysfunction and synaptic loss.

DISCLOSURE

This project was funded by the MIND-MAPS consortium. Ayla Mansur, Eugenii Rabiner, Yvonne Lewis, Mickael Huiban, Jan Passchier, and Roger Gunn are employees of Invicro LLC; Robert Comley is an employee of AbbVie; Roger Gunn is a consultant for AbbVie, Biogen, and Cerveau. Hideo Tsukada is an employee of Hamamatsu Photonics. No other potential conflict of interest relevant to this article was reported.

ACKNOWLEDGMENTS

We thank Elbert Perez, Ryan Janisch, and Mark Tanner for their expert assistance. We also thank the Yale University PET Center for providing the centrum semiovale regional definition.

The MIND-MAPS Consortium includes Laurent Martarello, Biogen; Robert A. Comley, AbbVie; Laigao Chen, Pfizer; Adam Schwarz, Takeda; Karl Schmidt, Celgene; Paul Matthews, Imperial College London; Marios Politis, King's College London; Jonathan Rohrer, University College London; David Brooks, Newcastle University; James Rowe, University of Cambridge; and the authors of this article.

KEY POINTS

QUESTION: What are the optimal kinetic modeling methods and outcome parameters for quantifying MC1, σ1R, and SV2A density as an index of mitochondrial/ER/synaptic axis function in the healthy human brain?

PERTINENT FINDINGS: In a cohort of 12 healthy volunteers who underwent a structural MRI scan and 90-min dynamic PET scans with ^{18}F-BCPP-EF, ^{11}C-SA-4503, and ^{11}C-UCB-J, the MA1 and 2TC models best described the kinetics of ^{18}F-BCPP-EF. Reliable quantification of ^{11}C-SA-4503 was achieved using MA1, whereas both 1TC and MA1 were suitable for ^{11}C-UCB-J quantification.

IMPLICATIONS FOR PATIENT CARE: The methods established here can be applied to patient cohorts assessing the same 3 ligands to potentially stratify patients or monitor the progression of molecular neuropathology.

REFERENCES

1. Grimm A, Eckert A. Brain aging and neurodegeneration: from a mitochondrial point of view. *J Neurochem.* 2017;143:418–431.
2. Xiang C, Wang Y, Zhang H, Han F. The role of endoplasmic reticulum stress in neurodegenerative disease. *Apoptosis.* 2017;22:1–26.
3. Briggs CA, Chakroborty S, Stutzmann GE. Emerging pathways driving early synaptic pathology in Alzheimer's disease. *Biochem Biophys Res Commun.* 2017;483:988–997.
4. Sazanov LA. A giant molecular proton pump: structure and mechanism of respiratory complex I. *Nat Rev Mol Cell Biol.* 2015;16:375–388.
5. Harada N, Nishiyama S, Kanazawa M, Tsukada H. Development of novel PET probes, [^{18}F]BCPP-EF, [^{18}F]BCPP-BF, and [^{11}C]BCPP-EM for mitochondrial complex 1 imaging in the living brain. *J Labelled Comp Radiopharm.* 2013;56:553–561.
6. Tsukada H. The use of ^{18}F-BCPP-EF as a PET probe for complex i activity in the brain. *Methods Enzymol.* 2014;547:417–431.
7. Tsukada H, Ohba H, Kanazawa M, Kakiuchi T, Harada N. Evaluation of ^{18}F-BCPP-EF for mitochondrial complex 1 imaging in the brain of conscious monkeys using PET. *Eur J Nucl Med Mol Imaging.* 2014;41:755–763.
8. Hayashi T, Su TP. Sigma-1 receptor chaperones at the ER-mitochondrion interface regulate Ca(2+) signaling and cell survival. *Cell.* 2007;131:596–610.
9. Su TP, Hayashi T, Maurice T, Buch S, Ruoho AE. The sigma-1 receptor chaperone as an inter-organelle signaling modulator. *Trends Pharmacol Sci.* 2010;31:557–566.
10. Nguyen L, Lucke-Wold BP, Mookerjee S, Kaushal N, Matsumoto RR. Sigma-1 receptors and neurodegenerative diseases: Towards a hypothesis of sigma-1 receptors as amplifiers of neurodegeneration and neuroprotection. *Adv Exp Med Biol.* 2017;964:133–152.
11. Francardo V, Bez F, Wieloch T, Nissbrandt H, Ruscher K, Cenci MA. Pharmacological stimulation of sigma-1 receptors has neurorestorative effects in experimental parkinsonism. *Brain.* 2014;137:1998–2014.
12. Jansen KLR, Faull RLM, Storey P, Leslie RA. Loss of sigma binding sites in the CA1 area of the anterior hippocampus in Alzheimer's disease correlates with CA1 pyramidal cell loss. *Brain Res.* 1993;623:299–302.
13. Sakata M, Kimura Y, Naganawa M, et al. Mapping of human cerebral sigma1 receptors using positron emission tomography and [^{11}C]SA4503. *Neuroimage.* 2007;35:1–8.
14. Mishina M, Ishiwata K, Ishii K, et al. Function of sigma1 receptors in Parkinson's disease. *Acta Neurol Scand.* 2005;112:103–107.
15. Mishina M, Ohyama M, Ishii K, et al. Low density of sigma1 receptors in early Alzheimer's disease. *Ann Nucl Med.* 2008;22:151–156.
16. Wan QF, Zhou ZY, Thakur P, et al. SV2 Acts via presynaptic calcium to regulate neurotransmitter release. *Neuron.* 2010;66:884–895.
17. Nowack A, Yao J, Custer KL, Bajjalieh SM. SV2 regulates neurotransmitter release via multiple mechanisms. *Am J Physiol Cell Physiol.* 2010;299:C960–C967.
18. Selkoe DJ. Alzheimer's disease is a synaptic failure. *Science.* 2002;298:789–791.
19. Reddy PH, Tripathi R, Troung Q, et al. Abnormal mitochondrial dynamics and synaptic degeneration as early events in Alzheimer's disease: Implications to mitochondria-targeted antioxidant therapeutics. *Biochim Biophys Acta.* 2012;1822:639–649.
20. Milnerwood AJ, Raymond LA. Early synaptic pathophysiology in neurodegeneration: Insights from Huntington's disease. *Trends Neurosci.* 2010;33:513–523.
21. Finnema SJ, Nabulsi NB, Eid T, et al. Imaging synaptic density in the living human brain. *Sci Transl Med.* 2016;8:348ra96.
22. Carson R, Naganawa M, Matuskey D, et al. Age and sex effects on synaptic density in healthy humans as assessed with SV2A PET [abstract]. *J Nucl Med.* 2018;59(suppl):541.
23. Chen M-K, Mecca AP, Naganawa M, et al. Assessing synaptic density in Alzheimer Disease with synaptic vesicle glycoprotein 2A positron emission tomographic imaging. *JAMA Neurol.* 2018;75:1215–1224.
24. Kawamura K, Ishiwata K, Tajima H, et al. In vivo evaluation of [^{11}C]SA4503 as a PET ligand for mapping CNS sigma1receptors. *Nucl Med Biol.* 2000;27:255–261.
25. Nabulsi NB, Mercier J, Holden D, et al. Synthesis and preclinical evaluation of ^{11}C-UCB-J as a PET tracer for imaging the synaptic vesicle glycoprotein 2A in the brain. *J Nucl Med.* 2016;57:777–784.
26. Jenkinson M, Pechaud M, Smith S. BET2: MR-based estimation of brain, skull and scalp surfaces. Presented at: 11th Annual Meeting of the Organization for Human Brain Mapping; June 12–16, 2005; Toronto, Ontario, Canada.
27. Grabner G, Janke AL, Budge MM, Smith D, Pruessner J, Collins DL. Symmetric atlasing and model based segmentation: an application to the hippocampus in older adults. Med Image Comput Comput Assist Interv. 2006;9:58-66.
28. Tziortzi AC, Searle GE, Tzimopoulou S, et al. Imaging dopamine receptors in humans with [^{11}C]-(+)-PHNO: Dissection of D3 signal and anatomy. *Neuroimage.* 2011;54:264–277.
29. Tzourio-Mazoyer N, Landeau B, Papathanassiou D, et al. Automated anatomical labeling of activations in SPM using a macroscopic anatomical parcellation of the MNI MRI single-subject brain. *Neuroimage.* 2002;15:273–289.
30. Ichise M, Toyama H, Innis RB, Carson RE. Strategies to improve neuroreceptor parameter estimation by linear regression analysis. *J Cereb Blood Flow Metab.* 2002;22:1271–1281.
31. Akaike H. Information theory and an extension of the maximum likelihood principle. *Int Symp Inf Theory.* 1973:267–281.
32. Ramakrishnan NK, Visser AK, Rybczynska AA, et al. Sigma-1 agonist binding in the aging rat brain: a MicroPET study with [(11)C]SA4503. *Mol Imaging Biol.* 2016;18:588–597.
33. Koole M, van Aalst J, Devrome M, et al. Quantifying SV2A density and drug occupancy in the human brain using [^{11}C]UCB-J PET imaging and subcortical white matter as reference tissue. *Eur J Nucl Med Mol Imaging.* 2019;46:396–406.
34. Finnema SJ, Nabulsi NB, Mercier J, et al. Kinetic evaluation and test–retest reproducibility of [^{11}C]UCB-J, a novel radioligand for positron emission tomography imaging of synaptic vesicle glycoprotein 2A in humans. *J Cereb Blood Flow Metab.* 2018;38:2041–2052.